Qualification of a Null Lens Using Image-Based Phase Retrieval

Matthew R. Bolcar[*], David L. Aronstein, Peter C. Hill, J. Scott Smith, Thomas P. Zielinski

NASA Goddard Space Flight Center, 8800 Greenbelt Rd., Greenbelt, MD 20771

ABSTRACT

In measuring the figure error of an aspheric optic using a null lens, the wavefront contribution from the null lens must be independently and accurately characterized in order to isolate the optical performance of the aspheric optic alone. Various techniques can be used to characterize such a null lens, including interferometry, profilometry and image-based methods. Only image-based methods, such as phase retrieval, can measure the null-lens wavefront in situ – in single-pass, and at the same conjugates and in the same alignment state in which the null lens will ultimately be used – with no additional optical components. Due to the intended purpose of a null lens (e.g., to null a large aspheric wavefront with a near-equal-but-opposite spherical wavefront), characterizing a null-lens wavefront presents several challenges to image-based phase retrieval: Large wavefront slopes and high-dynamic-range data decrease the capture range of phase-retrieval algorithms, increase the requirements on the fidelity of the forward model of the optical system, and make it difficult to extract diagnostic information (e.g., the system F/#) from the image data. In this paper, we present a study of these effects on phase-retrieval algorithms in the context of a null lens used in component development for the Climate Absolute Radiance and Refractivity Observatory (CLARREO) mission. Approaches for mitigation are also discussed.

Keywords: phase retrieval, null lens test, asphere metrology

1. INTRODUCTION

1.1 CLARREO

The Climate Absolute Radiance and Refractivity Observatory (CLARREO)[1] is a mission developed by NASA and partner organizations for a future climate observing system. In support of the CLARREO mission, NASA's Goddard Space Flight Center (GSFC) has designed and built an all-aluminum imaging spectrometer called the "Solar, Lunar for Absolute Reflectance Imaging Spectroradiometer" (SOLARIS). The SOLARIS instrument is a science demonstration unit that will be used to evaluate the feasibility of achieving the 0.3% radiometric measurement accuracies required for the CLARREO mission.

The design of the SOLARIS instrument is a three-mirror telescope (TMT) imager in series with an Offner spectrometer. Figure 1 shows the optical layout of the design. The instrument has a 10° field-of-view and operates in the wavelength band from 320 nm to 2.3 μm. Each optical surface was manufactured by a diamond-turning process, resulting in a figure accuracy of 0.05 waves RMS and a surface finish of 20 Å. The TMT uses two aspheric surfaces—one a hyperboloid and the other an oblate spheroid.

Two independent computer-generated holograms (CGHs) were used to measure the optical figure error of the two aspheres after diamond turning. A Hindle sphere test and a null-lens test were also performed as crosschecks to the CGH tests. It is important to realize that both the CGH tests and null-lens test measure a wavefront that is a composite of the test-hardware wavefront and that of the system under test. It is critical that the CGH and the null lens are accurately characterized so that their contribution to the measured wavefront can be removed. It is the characterization of the null lens with image-based phase retrieval that is the focus of this paper.
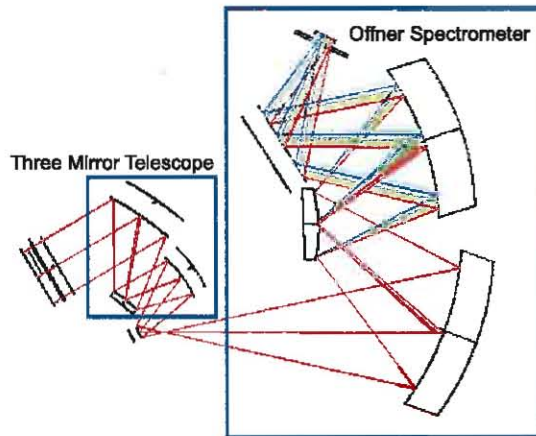
[*] matthew.bolcar@nasa.gov

Figure 1 – The CLARREO SOLARIS Instrument, consisting of a three-mirror telescope and Offner spectrometer in series.

1.2 Null lens design

Null lenses are used to test the figure of an asphere during optical fabrication. They must be custom designed to null the reflected or transmitted wavefront of the aspheric optic under test. For high-numerical-aperture aspheric optics, the design of the null lens becomes more complex, often requiring two or more custom optical components to be precision-aligned to one another, as well as to a reference source and the aspheric surface under test. Using catalog, off-the-shelf (COTS) lenses, it is possible to design multi-element null lenses that are capable of measuring the figure error of off-axis aspheric optical elements with speeds greater than F/1. Using COTS lenses offers a technically viable, time efficient, and cost effective setup for asphere metrology.

Prior to assembling the null lens, the radius, figure, and thickness of each COTS lens were measured. Lens spacers were custom designed to compensate for the manufacturing errors present in each lens and the lens clocking was optimized to reduce wavefront error in the final null-lens test configuration.
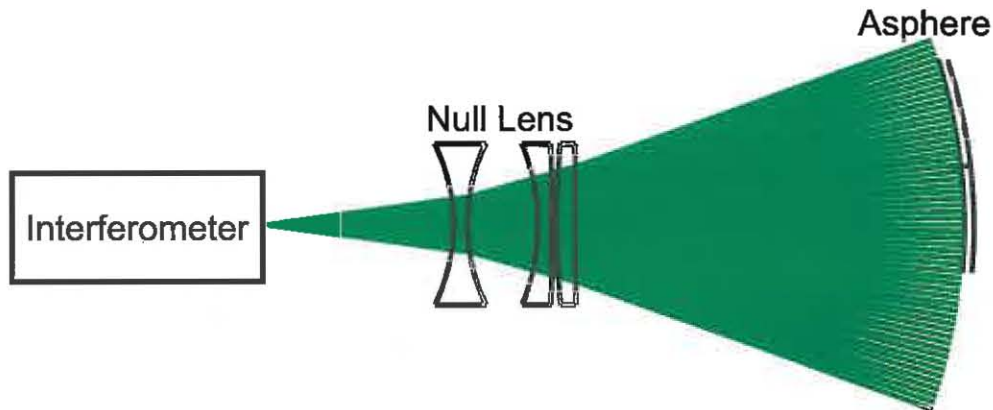

Figure 2 - Asphere metrology test setup. An interferometer provides a diverging spherical beam that the null lens corrects to match the asphere being tested.

Figure 2 shows the optical layout of the null-lens test used to measure the figure error of the oblate spheroid in the SOLARIS instrument. Alignment of the null-lens test was accomplished by first aligning the null lens to the interferometer source. Since the first surface of the null lens is concentric about the interferometer source, the ghost of the first surface was used to align the null lens to the interferometer optically. This ghost fringe does not impact the asphere figure measurement, because the intensities between the glass lens reflection and the metal mirror reflection are

significantly different. After the null lens has been aligned to the interferometer, the asphere is aligned to the null lens using a metering structure.

1.3 Null lens test using phase retrieval

Phase retrieval (also called image-based wavefront sensing) is a method for determining the wavefront of an optical element or system. Unlike other techniques for characterizing optical wavefronts (such as using an interferometer or a Shack-Hartmann wavefront sensor), phase retrieval can test an optical system with minimal additional opto-mechanical hardware — light can pass through the optical system in its as-used configuration and images can be recorded using the system's own detector[2].

The primary data used by phase retrieval to determine the optical wavefront is a set of images collected using the optical system under test. Rather than simply recording the same image repeatedly (which would serve to reduce the signal-to-noise ratio), it is preferred to take a set of *diverse* images — with some aspect of the test setup varied systematically between images. In the null-lens qualification described in the present paper, *defocus diversity* was implemented; images were taken having different amounts of defocus by scanning the detector along the optical axis in 5-mm increments between recorded images.

The phase-retrieval process requires an accurate *forward model* that describes the propagation of light through the optical system and its detection at the focal plane. Details about the optical system — including the spectrum of the illumination, the intensity profile of the beam, the speed of the beam at the detector, the geometry of the pupil stop, the detector pixel size, and the noise characteristics of the detector — contribute to an accurate forward model. Broadly speaking, the better the knowledge of these parameters & details, the smaller the uncertainty in the wavefront that is estimated by phase retrieval. There is typically some level of uncertainty in all of these parameters an in other aspects of the test setup, however the phase-retrieval process can usually reduce the uncertainty in these parameters in the course of recovering the system's wavefront.

There are two key advantages to using phase retrieval to qualify the null lens:
- Traditional interferometric tests require a retroreflector to retrace the path through the test optic, creating a double-pass test of the lens. Double-pass tests are prone to retrace errors (where the first pass and second pass do not take identical paths through the lens). Phase retrieval does not require a retroreflector and performs a single-pass test of the lens, eliminating retrace errors as well as wavefront contributions from the retroreflector.
- The null lens can be tested *in situ*, using the same conjugate and alignment as in actual use. Although the systematic errors introduced by off-conjugate testing can largely be modeled and the results corrected, the uncertainties in inter-element distances and in indexes of refraction can propagate to an unnecessarily large final uncertainty in the optical wavefront. The null lens tested here has many waves departure from a reference spherical wavefront and that wavefront is sensitive to its orientation with the rest of the optical system, so qualifying it *in situ* is critical to determining if the null lens was manufactured to within its tight wavefront budget.

There are also two disadvantages to using phase retrieval to qualify the null lens:
- The null lens has multiple waves of wavefront departure and also has a large wavefront slope across the optical system's exit pupil. The large wavefront departure leads to large images formed on the detector, spanning hundreds of detector pixels in each direction, even at best focus. The large wavefront slope further requires that the phase-retrieval simulations be performed using a high-resolution model of the optical system's exit pupil. Both of these issues require large amounts of computer memory to be used to perform the phase retrievals, increasing the amount of time required to manipulate the large datasets and estimate wavefront. Note that large wavefront error can lead to challenges in phase retrieval that are analogous to the problems of high fringe density in interferometry[3].
- The null lens creates a relatively fast beam (~F/7), making the system sensitive to the orientation of the light source relative to the null lens, and sensitive to the orientation of the null lens relative to the detector. The small placement uncertainties in aligning the optical system and test set-up (typically < 1mm) are still large enough to compromise the fidelity of the forward model used in phase retrieval.

1.4 Outline of the Paper

In Section 2, we present an overview of the phase-retrieval process and what is typically required for an accurate estimation of a system's wavefront. Section 3 describes the specific challenges that testing the SOLARIS TMT null lens presents to the phase-retrieval process, and how those challenges dictated our approach to estimating the wavefront. In Section 4 we describe the test setup and show example data. In Section 5 we present phase-retrieval results and conclude in Section 6.

2. IMAGE-BASED PHASE RETRIEVAL

2.1 Overview

The phase retrieval process uses computer simulations of light traveling through the optical system and arriving at the light detector (as described by the forward model), and the computer algorithm determines the optical wavefront that is most consistent with the set of diverse images recorded by the detector. There are two general categories of phase-retrieval algorithms: In *iterative-transform* algorithms (based on the Misell-Gerchberg-Saxton algorithm)[4], light is simulated traveling back and forth through the optical system — from the exit pupil of the optical system to the light detector, and then backwards from the detector to the exit pupil — repeatedly until the algorithm converges. At each destination (first at the detector, and then at the exit pupil), the amplitude of the light field is replaced with data from optical models or measurements while leaving the phase (the wavefront) untouched[5]. In *non-linear optimization* algorithms, only the forward propagation (from the exit pupil to the detector) is simulated, and then the images predicted by the simulation are compared to the measured images using a scalar metric, often based on a normalized root-mean-squared error between simulation and measurements. The scalar metric is minimized with respect to the wavefront in the exit pupil[6,7]. Both algorithm approaches were applied to qualifying the SOLARIS null lens.

The forward model used in this phase-retrieval study propagates the electric field using a two-step process:
- Light is propagated a distance z, from the null-lens pupil (having diameter D) to the location in image space of "best focus," here defined as where the defocus component of the optical wavefront vanishes. This propagation is implemented using the Fresnel approximation to the integral (propagator) solutions to the Helmholtz wave equation[8].
- Light is then propagated from "best focus" to by a distance δz to reach the nearest plane of measured data using the angular spectrum (plane wave) representation of the field. From here, the light is again propagated using the angular spectrum method by various distances, Δz_k, to the locations where the detector was placed to record images[8].

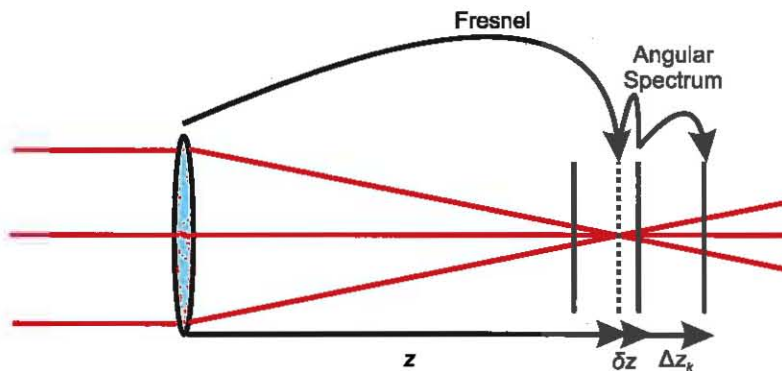A schematic of this two-step process is shown in Figure 3.

Figure 3 – The two-step propagation technique. A Fresnel propagation takes the field in the pupil of the optical system to focal plane of the system (dotted line). From there, an angular spectrum method is used to propagate the field about the nominal focal plane to the various measurement planes (solid lines). First, a small corrective step, δz, is taken to propagate the best-focus field to the nearest measurement plane. Then, the field is propagated to the desired measurement plane by a distance Δz_k.

An important consideration in designing a phase-retrieval measurement and in simulating the forward model is the *sampling* of the light intensity by the light detector. The sampling ratio Q is defined by

$$Q = \frac{\lambda \left(\frac{F}{\#} \right)}{\Delta u} \quad (1)$$

where λ is the wavelength of light, $F/\#$ is the ratio of the distance of propagation, z, to focus to the pupil diameter, D, and Δu is the spacing of detector pixels. A sampling ratio of $Q = 2$ represents a critically sampled light intensity, in the sense of the Nyquist Sampling Theorem.

In our experimental set-up, described below, the wavelength λ, the pixel spacing Δu, and the pupil diameter D are well known, but the propagation distance z is sensitive to the null-lens alignment along the optical axis. Our initial uncertainty in this propagation distance z maps to a corresponding uncertainty in the sampling ratio Q. As discussed below, this uncertainty in z and Q proved to be one of the challenges of determining the null-lens wavefront.

2.2 Methods for Improving Uncertainties

Although the method used to determine the null-lens wavefront is commonly called "phase retrieval," it is also a framework for retrieving — estimating, or improving our knowledge of the values and uncertainties — other aspects that describe the optical system. The key additional retrievals considered in the present study are discussed below:

Detector-position uncertainty: The two-step forward model described above was designed to determine the optical wavefront in the plane of zero defocus. If the phase-retrieval algorithm retrieves Zernike defocus in the optical system wavefront, it is a signal that the distances, Δz_k, along the optical axis (where the detector was placed) are not accurate. Knowledge of these distances can be improved by directly optimizing their values in nonlinear optimization, or by using the sensed defocus in a "feedback loop". The defocus coefficient of fringe Zernike Z_4 and the position correction Δz are paraxially related by:

$$Z_4 = \frac{1}{16} \frac{D^2 \Delta z}{z(z + \Delta z)} \quad (2)$$

Sampling ratio Q: Images formed from hard-edged pupils have a sharp cutoff in their spatial frequencies. This fact can be used to determine the sampling by examining the spatial frequencies of the images, using the modulation transfer function (MTF). Techniques have been developed to improve knowledge of Q during phase retrieval[9,10].

Intensity profile of the beam: The light profile in the optical system's pupil can also be estimated by allowing both the amplitude and the phase to be optimized during retrieval[7,11,12].

Broadly speaking, in order to meaningfully retrieve multiple aspects of the optical system, the diverse set of images used must be large and diverse enough to allow for sensing of all of these different quantities. In short, this is why numerous diverse images are desired as input to the retrieval process.

3. CHALLENGES OF TESTING THE NULL LENS

3.1 Optical Model

It is common to use an optical model (describing the optical system being tested) both to design the phase-retrieval test itself and to provide first estimates for the parameters needed in the forward model. Such an optical model of the phase-retrieval test of the SOLARIS null lens was developed using Radiant Zemax's *Zemax* software[13]. The optical model started with the nominal design of the three-element null lens, and then as-fabricated surfaces were added by incorporating interferometric measurements of surface wavefronts into the model using a Zernike-polynomial fit to metrology data.

The model predicts that the F/# at the detector is approximately 7.3. In testing the null lens at a wavelength of 632.8 nm, using a detector with 2.2 μm-square pixels, the sampling ratio is $Q = 2.09$.

The model predicts that the null lens should have −7.23 waves of 3rd order spherical aberration, the dominant aberration of the lens used at this conjugate. Although it is the job of the phase-retrieval algorithm to find the wavefront most consistent with the measured image data, the method is most successful if you have a starting estimate of the wavefront that is accurate to ~1 wave (PV), so this model prediction was used as a starting point for analysis.

The large amount of spherical aberration led to two challenges in bridging between the optical model and the measured data in order to get good estimates of parameters for phase retrieval:

First, the optical model predicts that the wavefront from the null lens is sensitive to the distance between the transmission sphere and the front of the null lens (see Figure 6), a distance that could only be measured to ~1 mm. This sensitivity made it challenging to predict a good estimate of the 3rd order spherical aberration.

Second (although coupled to the first point above), optical systems with large spherical aberration have several distinct locations of "best focus", including paraxial best focus, zero defocus position, and smallest RMS spot size, that are almost coincident in systems with more modest wavefront errors. It is hard to use the optical model to accurately estimate the propagation distance z needed in the forward model, and this distance doesn't have a clear "signal" so that it can be determined experimentally by monitoring image characteristics in different locations of the detector.

The Zemax optical model was also used to simulate the data we expected to measure in the laboratory experiment, and that exercise uncovered two other unanticipated issues that further compounded the analysis difficulties:

First, this large amount of spherical aberration leads to high-dynamic-range images near best focus (see Figure 4). That is, the light intensity falls off away from the center of the PSF rapidly, and the rings of the PSF are 2.5 orders-of-magnitude more dim than the core. Since detector measurements are converted into digital information (having a 12-bit range for the detector used in this experiment), this issue makes it challenging to have the entire image be unsaturated and have a good signal-to-noise ratio (SNR). From this modeling, we decided to take two different types of images for each defocus-diversity measurement — one that properly exposes the center of the PSF and thus under-exposes the wings, and one that saturates the center and properly exposes the wings.
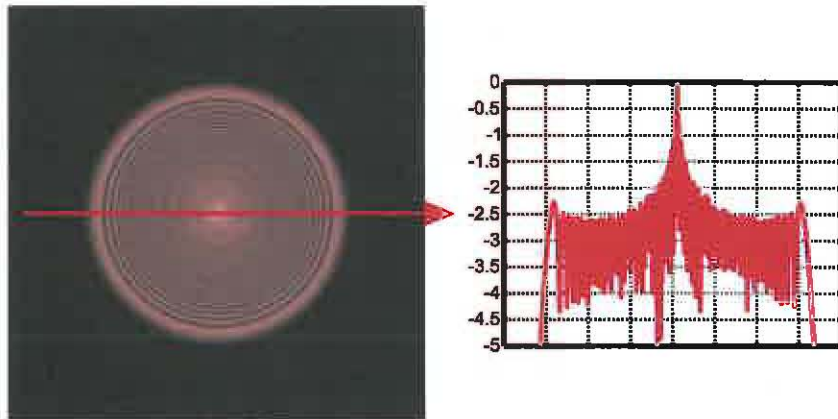

Figure 4 – Illustration of high dynamic range in a simulated PSF. On the right is a log-scale plot of a slice across the PSF. The rings of the PSF are 2.5 orders-of-magnitude less intense than the peak.

Second, this amount of spherical aberration also leads to high-dynamic-range features in the MTFs of the images. Recall that MTFs of images formed from hard-edged pupils show a sharp cut-off at a maximum spatial frequency, and estimating this cut-off in measured images is a powerful tool in refining knowledge of the optical system's $F/\#$ (and thus the sampling ratio Q) at the detector. The Zemax models predicts that these high-spherical-aberration images look like they have a cut-off at one frequency (see Figure 5(a)) but when using a larger amount of logarithmic stretching, it becomes clear that the true cut-off appears at higher spatial frequencies (see Figure 5(b)). Our concern was that this true cut-off would be hard to discern in measured data, even with good image SNR, and that the use of the MTF to estimate the $F/\#$ would be less effective than it is in lower-aberration systems.
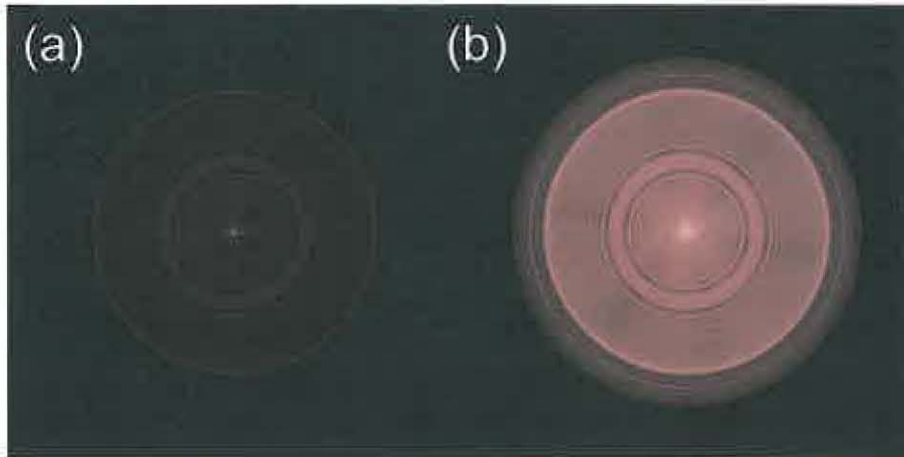
Figure 5 – Illustration of the high-dynamic range in the MTF of simulated data. In (a), an initial stretching of the MTF masks the faint outer ring that is seen in (b) after further stretching, hiding the true cutoff frequency of the optical system. For real, noisy data, this outer ring may be hidden in noise, making estimation of the sampling Q and system $F/\#$ difficult.

3.2 Quadratic Optical Model & Grid Search

The two-step propagation technique described in Section 2.1 requires three quantities to accurately take the field in the pupil of the system to each of the measurement planes: the propagation distance, z, the data offset, δz, and the defocus plane separation, Δz_k (see Figure 3). It is important to note that the propagation distance also determines the F/#, and therefore the sampling Q of the data via Eq. (1).

The stage that was used to move the camera through focus is accurate to within a few microns, implying that the plane separation, Δz_k, is comparatively well known. The uncertainty in the propagation distance and the data offset, however, is linked to an uncertainty in two separate distances in the optical setup. As described in Section 4, the distance between the transmission sphere and the null lens and the distance between the null lens and the detector plane both have errors on the order of ± 1 mm. The optical model indicates that such errors can change the propagation distance by ~20% and the magnitude of the predicted wavefront by ~8% — enough to push the phase-retrieval algorithm outside of its capture range.

A grid search was performed to help refine the prior knowledge of z and δz. For a given distance, z, the wavefront was propagated using the Fresnel propagator with the appropriate sampling Q. The resulting field was then propagated using the angular spectrum technique by the offset distance, δz, to correspond to one of the measurement planes, which we will arbitrarily call the "best-focus" plane. This is the measurement plane that most closely corresponds to having zero defocus in the pupil of the optical system. From the best-focus plane, the field was propagated using the angular-spectrum method by distances in increments of $\pm \Delta z_k$ to reach the other measurement planes. In each plane, the normalized root-mean-squared-error (NRMSE) was computed between the simulated PSF and the measured PSF using a metric that insensitive to bias, gain and translation[14,15]. A range of values of z and δz was evaluated to find the optimal values that simultaneously minimized the NRMSE in all of the measurement planes.

One additional quantity is required to complete this process: the wavefront to be propagated. Indeed, that is the very quantity that the entire experiment seeks to determine. For the purposes of this grid search, though, a reasonably good approximation to the wavefront will suffice. The optical model predicts that, by far, the two dominant terms in the wavefront are 3rd and 5th order spherical aberration (Z_9 and Z_{16} in the Fringe Zernike ordering, respectively), and values of these coefficients are dependent on the distance between the transmission sphere and the null lens, z_{tn}.

To mitigate this effect, the optical model was queried with different values of z_m and the resulting propagation distance and 3rd and 5th order spherical aberration values were recorded. A quadratic least squares fit was performed to determine an empirical relationship between each of the aberration terms and the propagation distance. Thus, as the propagation distance was varied during the grid search, an estimate of the wavefront in the pupil consisting only of 3rd and 5th order spherical was generated.

Ultimately, the optimal values for z and δz, and the corresponding coefficients for Z_9 and Z_{16} were then used as the starting point for the phase-retrieval algorithm.

4. DATA COLLECTION

4.1 Test Setup

Recall that Figure 2 shows the optical design of how the null lens will be used to test the oblate spheroid of the SOLARIS system. Figure 6 shows the optical design of how the phase-retrieval data was collected to test the null lens itself.
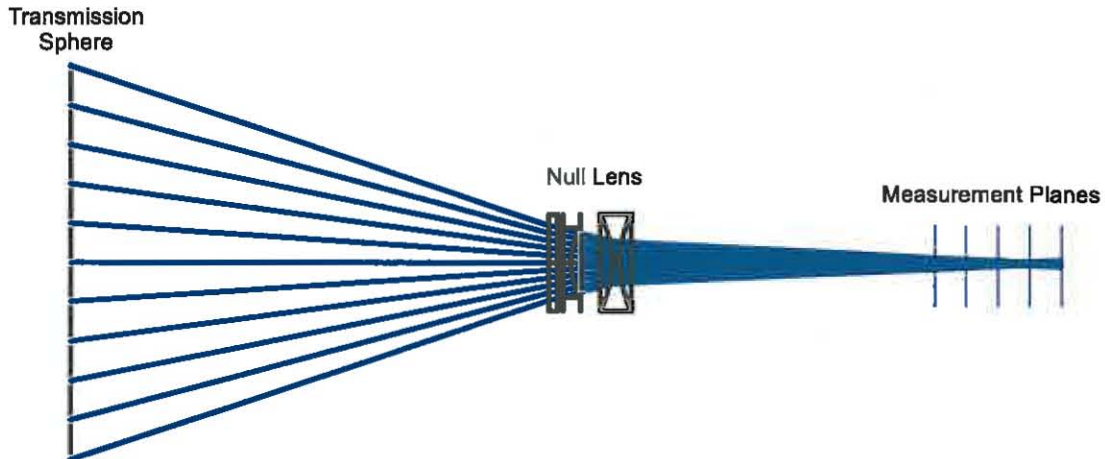

Figure 6 – Phase retrieval test setup for characterizing the null lens. An F/1.5 transmission sphere provides a converging spherical beam to the null lens. The detector is swept through a range the spans paraxial best-focus to marginal best-focus. Note that the transmission sphere is the stop of the system and therefore is also the entrance pupil.

An interferometer fitted with an F/1.5 transmission sphere provides a converging beam to the null lens. A reflection from a buried surface in the null lens was used to help align the null lens to the interferometer by minimizing the number of fringes as viewed by the interferometer.

The detector is swept along the optical axis in 5-mm increments, over a range that approximately spans the distance between paraxial best focus and marginal best focus. Figure 7 shows a photo of the actual setup.
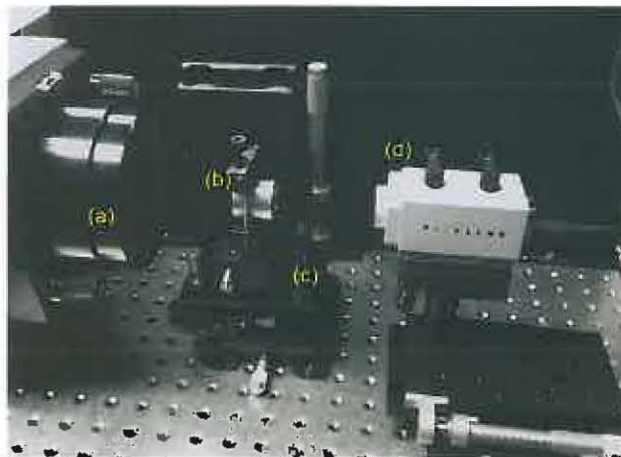

Figure 7 – Photo of the test setup. The transmission sphere (a) provides a converging spherical beam to the null lens being tested (b). A thin, Wratten ND filter (c) is used to reduce the intensity of the beam before it is detected by the camera (d).

4.2 Example Data

Figure 8 shows the measured PSFs in each plane. Figure 9 shows the MTF that corresponds to each measurement plane. Note that the faint cutoff that is seen in the simulated MTFs is not seen in the measured data, implying that one might infer the wrong sampling Q from the data.

Figure 8 – The measured PSFs. The left-most image was collected at approximately paraxial best focus. The right-most image was collected at approximately marginal best focus. The distance between each data plane is 5 mm.

Figure 9 – The MTFs computed from the measured PSFs. Note that the fainter outer edge of the cutoff seen in Figure 5 is not visible here.

5. RESULTS

Figure 10 shows the retrieved PSFs, and reports the value of the NRMSE for each one.

| 0.0444 | 0.1185 | 0.1958 | 0.2668 | 0.2728 | 0.2317 | 0.2098 |

Figure 10 – The retrieved PSFs. The NRMSE between the retrieved and measured PSF is also reported for each plane.

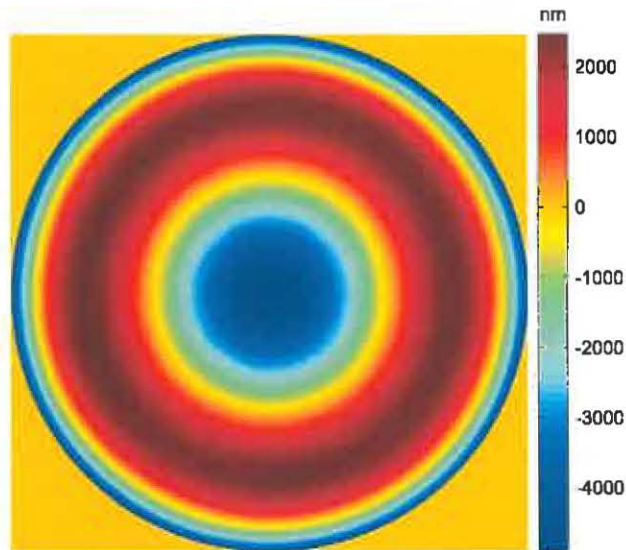Figure 11 shows the estimated wavefront in the pupil of the system. The total RMS wavefront error is 2.1 μm.

Figure 11 – The estimated wavefront. The RMS value is 2.1 μm.

Figure 12(a) shows the predicted wavefront from the Zemax model, and Figure 12(b) shows the difference between the estimated and predicted wavefronts. This difference has an RMS value of 51 nm, after the dominant aberration terms of focus, 3rd and 5th order spherical are removed.
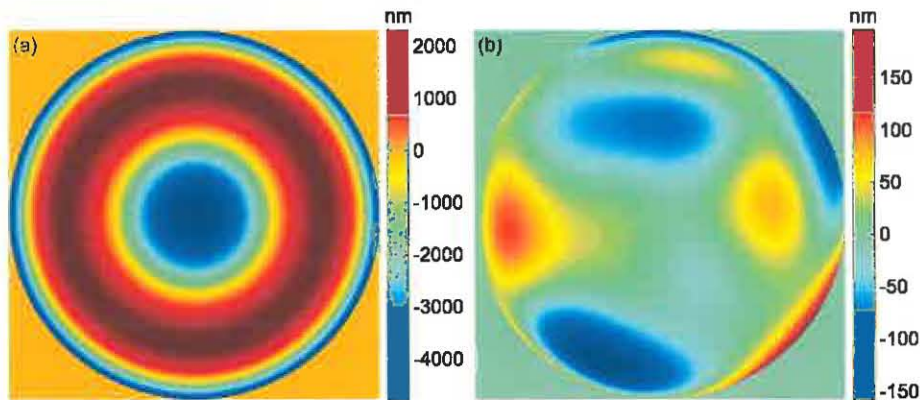

Figure 12 – (a) The wavefront predicted by the optical model in Zemax. (b) The difference between estimated wavefront and the predicted wavefront. The RMS difference is 50 nm.

6. CONCLUSION

We presented here the results of an effort to characterize a null lens using image-based phase retrieval. The null lens was design as a back-up test to one of the two aspheric mirrors in the SOLARIS instrument.

Several unanticipated challenges presented themselves during the course of the effort, including a large uncertainty in some of the basic first-order optical properties that are required to generate an accurate forward model for the phase-retrieval algorithm. Furthermore, the large amount of spherical aberration present in the system lead to a high dynamic range in both the collected data PSFs and the computed MTFs, limiting the ability to estimate the unknown optical properties using established techniques.

A grid-search technique that leveraged a quadratic optical model was used to help reduce the uncertainty in the propagation distance, data offset and initial values of the dominant wavefront terms. Ultimately, the wavefront of the null lens was recovered and is in agreement with the predicted wavefront from an optical model by better than $1/12^{th}$ of a wave.

7. REFERENCES

[1] See: http://clarreo.larc.nasa.gov/

[2] Brady, G.R. and Fienup, J.R., "Phase retrieval as an optical metrology tool; Technical Digest," in *Optifab: Technical Digest, SPIE Technical Digest,* pp. 139-141 (2005).

[3] Brady, G.R. and Fienup, J.R., "Measurement range of phase retrieval in optical surface and wavefront metrology," *Appl. Opt.* 48, 442-449 (2009).

[4] Gerchberg, R.W. and Saxton, W.O., "A practical algorithm for the determination of phase from image and diffraction plane pictures," *Optik* 35, 237-246 (1972).

[5] Dean, B.H., Aronstein, D.L., Smith, J.S., Shiri, R., and Acton, D.S., "Phase retrieval algorithm for JWST Flight and Testbed Telescope," Proc. SPIE 6265, 626511 (2006).

[6] Fienup, J.R., "Phase-retrieval algorithms for a complicated optical system," *Appl. Opt.* 32, 1737-1746 (1993).

[7] Thurman, S.T. and Fienup, J.R., "Complex pupil retrieval with undersampled data," *J. Opt. Soc. Am. A* 26, 2640-2647 (2009).

[8] Goodman, J.W., *Introduction To Fourier Optics, 3rd Ed* (Roberts & Co, 2005).

[9] Zielinski, T. P., Dean, B. H., Smith, J. S., Aronstein, D. L., and Fienup, J. R., "Determination of the Sampling Factor in a Phase-Diverse Phase Retrieval Algorithm," in *Frontiers in Optics*, OSA Technical Digest (CD) (Optical Society of America, 2010), paper FWJ3.

[10] Aronstein, D., and Smith, J. S., "Recovery of the Image-Plane Sampling Parameter Q within Iterative-Transform Phase Retrieval," in *Frontiers in Optics*, OSA Technical Digest (Optical Society of America, 2011), paper FThD6.

[11] Brady, G.R. and Fienup, J.R., "Nonlinear optimization algorithm for retrieving the full complex pupil function," *Opt. Express* 14, 474-486 (2006).

[12] Dean, B., "Optimization Algorithms for Phase and Pupil Amplitude Recovery," in *Frontiers in Optics*, OSA Technical Digest (Optical Society of America, 2011), paper FThK3.

[13] See: http://www.radiantzemax.com/en/design/

[14] Fienup, J.R., "Invariant error metrics for image reconstruction," *Appl. Opt.* 36, 8352-8357 (1997).

[15] Thurman, S.T. and Fienup, J.R., "Phase retrieval with signal bias," *J. Opt. Soc. Am. A* 26, 1008-1014 (2009).

# Qualification of a Null Lens Using Image-Based Phase Retrieval

Matthew R. Bolcar, David L. Aronstein, Peter C. Hill, J. Scott Smith, Thomas P. Zielinski
NASA Goddard Space Flight Center, 8800 Greenbelt Rd., Greenbelt, MD 20771

In measuring the figure error of an aspheric optic using a null lens, the wavefront contribution from the null lens must be independently and accurately characterized in order to isolate the optical performance of the aspheric optic alone. Various techniques can be used to characterize such a null lens, including interferometry, profilometry and image-based methods. Only image-based methods, such as phase retrieval, can measure the null-lens wavefront in situ — in single-pass, and at the same conjugates and in the same alignment state in which the null lens will ultimately be used — with no additional optical components. Due to the intended purpose of a null lens (e.g., to null a large aspheric wavefront with a near-equal-but-opposite spherical wavefront), characterizing a null-lens wavefront presents several challenges to image-based phase retrieval: Large wavefront slopes and high-dynamic-range data decrease the capture range of phase-retrieval algorithms, increase the requirements on the fidelity of the forward model of the optical system, and make it difficult to extract diagnostic information (e.g., the system F/#) from the image data. In this paper, we present a study of these effects on phase-retrieval algorithms in the context of a null lens used in component development for the Climate Absolute Radiance and Refractivity Observatory (CLARREO) mission. Approaches for mitigation are also discussed.

Introduction

The Climate Absolute Radiance and Refractivity Observatory (CLARREO) is a mission developed by NASA and partner organizations for a future climate observing system. In support of the CLARREO mission, NASA's Goddard Space Flight Center (GSFC) has designed and built an all-aluminum imaging spectrometer called the "Solar, Lunar for Absolute Reflectance Imaging Spectroradiometer" (SOLARIS). The SOLARIS instrument is a science demonstration unit that will be used to evaluate the feasibility of achieving the 0.3% radiometric measurement accuracies required for the CLARREO mission.

Figure 1 - The CLARREO SOLARIS instrument.
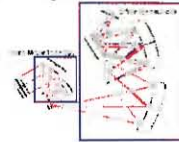
The design of the SOLARIS instrument is a three-mirror telescope (TMT) imager in series with an Offner spectrometer. The instrument has a 10° field-of-view and operates in the wavelength band from 320 nm to 2.3 μm. Each optical surface was manufactured by a diamond-turning process, resulting in a figure accuracy of 0.06 waves RMS and a surface finish of 20 Å. The TMT uses two aspheric surfaces—one a hyperboloid and the other an oblate spheroid.

Two independent computer-generated holograms (CGH) were used to measure the optical figure error of the two aspheres after diamond turning. A Hindle sphere test and a null-lens test were also performed as crosschecks to the CGH tests. It is important to realize that both the CGH tests and null-lens test measure a wavefront that is a composite of the test-hardware wavefront and that of the system under test. It is critical that the CGH and the null lens are accurately characterized so that their contribution to the measured wavefront can be removed. It is the characterization of the null lens with image-based phase retrieval that is the focus of this paper.

Image-based Phase Retrieval

The phase retrieval process uses computer simulations of light traveling through the optical system and arriving at the light detector (as described by a forward model), and the computer algorithm determines the optical wavefront that is most consistent with the set of diverse images recorded by the detector. There are two general categories of phase-retrieval algorithms: In iterative-transform algorithms (based on the Misell-Gerchberg-Saxton algorithm), light is simulated traveling back and forth through the optical system — from the exit pupil of the optical system to the light detector, and then backwards from the detector to the exit pupil — repeatedly until the algorithm converges. At each destination (first at the detector, and then at the exit pupil), the amplitude of the light field is replaced with data from optical models or measurements while leaving the phase (the wavefront) untouched. In non-linear optimization algorithms, only the forward propagation (from the exit pupil to the detector) is simulated, and then the images predicted by the simulation are compared to the measured images using a scalar metric, often based on a normalized root-mean-squared error between simulation and measurements. The scalar metric is minimized with respect to the wavefront in the exit pupil. Both algorithm approaches were applied to qualifying the SOLARIS null lens.

The forward model used in this phase-retrieval study propagates the electric field using a two-step process, illustrated in Figure 2:

- Light is propagated a distance z, from the null-lens pupil (having diameter D) to the location in image space of "best focus," here defined as where the defocus component of the optical wavefront vanishes. This propagation is implemented using the Fresnel approximation to the integral (propagator) solutions to the Helmholtz wave equation.

- Light is then propagated from "best focus" to by a distance δz to reach the nearest plane of measured data using the angular spectrum (plane wave) representation of the field. From here, the light is again propagated using the angular spectrum method by various distances, Δz, to the locations where the detector was placed to record images.

Figure 2 - The two-step propagation technique. A Fresnel propagation takes the field in the pupil of the optical system to focal plane of the system (dotted line). From there, an angular spectrum method is used to propagate the field about the nominal focal plane to the various measurement planes (solid lines). First, a small correction step, δz, is taken to propagate the best-focus field to the nearest measurement plane. Then, the field is propagated to the desired measurement plane by a distance Δz.
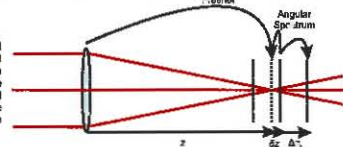
Challenges of Testing The Null Lens

It is common to use an optical model (describing the optical system being tested) both to design the phase-retrieval test itself and to provide first estimates for the parameters needed in the forward model. Such an optical model of the phase-retrieval test of the SOLARIS null lens was developed using Radiant Zemax's Zemax software. The optical model started with the nominal design of the three-element null lens, and then as-fabricated surfaces were added by incorporating interferometric measurements of surface wavefronts into the model using a Zernike-polynomial fit to metrology data.

The model predicts that the F/# at the detector is approximately 7.3. In testing the null lens at a wavelength of 632.8 nm, using a detector with 2.2 μm-square pixels, the sampling ratio is Q = 2.09. The model further predicts that the null lens should have ~7.23 waves of 3rd order spherical aberration, the dominant aberration of the lens used at this conjugate. The large amount of spherical aberration led to two challenges in bridging between the optical model and the measured data in order to get good estimates of parameters for phase retrieval:

First, the optical model predicts that the wavefront from the null lens is sensitive to the distance between the transmission sphere and the front of the null lens, a distance that could only be measured to ~1 mm. This sensitivity made it challenging to predict a good estimate of the 3rd order spherical aberration.

Second (although coupled to the first point above), optical systems with large spherical aberration have several distinct locations of "best focus", including paraxial best focus, zero defocus position, and smallest RMS spot size, that are almost coincident in systems with more modest wavefront errors. It is hard to use the optical model to accurately estimate the propagation distance z needed in the forward model, and this distance doesn't have a clear "signal" so that it can be determined experimentally by monitoring image characteristics in different locations of the detector.

The Zemax optical model was also used to simulate the data we expected to measure in the laboratory experiment, and that exercise uncovered two other unanticipated issues that further compounded the analysis difficulties:

First, this large amount of spherical aberration leads to high-dynamic-range images near best focus (see Figure 3). That is, the light intensity falls off away from the center of the PSF rapidly and the rings of the PSF are 2.5 orders-of-magnitude more dim than the core. Since detector measurements are converted into digital information (having a 12-bit range for the detector used in this experiment), this issue makes it challenging to have the entire image be unsaturated and have a good signal-to-noise ratio (SNR).
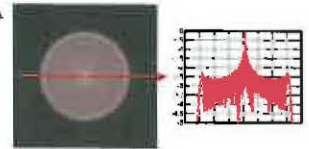

Figure 3 - Illustration of high dynamic range in a simulated PSF. On the right is a log-scale plot of a slice across the PSF. The rings of the PSF are 2.5 orders-of-magnitude less intense than the peak.

Second, this amount of spherical aberration also leads to high-dynamic-range features in the MTFs of the images. Recall that MTFs of images formed from hard-edged pupils show a sharp cut-off at a maximum spatial frequency, and estimating this cut-off in measured images is a powerful tool in refining knowledge of the optical system's F/# (and thus the sampling ratio Q) at the detector. The Zemax models predicts that these high-spherical-aberration images look like they have a cut-off at one frequency (see Figure 4(a)) but when using a larger amount of logarithmic stretching, it becomes clear that the true cut-off appears at higher spatial frequencies (see Figure 4(b)). Our concern was that this true cut-off would be hard to discern in measured data, even with good image SNR, and that the use of the MTF to estimate the F/# would be less effective than it is in lower-aberration systems.

Figure 4 - Illustration of the high-dynamic-range in the MTF of simulated data. In (a), an initial stretching of the MTF masks the faint outer ring that is seen in (b) after further stretching, hiding the true cutoff frequency of the optical system. For real, noisy data, this outer ring may be hidden in noise, making estimation of the sampling Q and system F/# difficult.

Data Collection

Figure 5 shows the optical design of how the phase-retrieval data was collected to test the null lens. An interferometer fitted with an F/1.5 transmission sphere provides a converging beam to the null lens. A reflection from a buried surface in the null lens was used to help align the null lens to the interferometer by minimizing the number of fringes as viewed by the interferometer. The detector is swept along the optical axis in 5-mm increments, over a range that approximately spans the distance between paraxial best focus and marginal best focus. Figure 6 shows a photo of the actual setup.
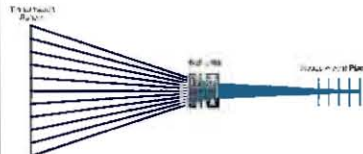

Figure 5 - Phase retrieval test setup for characterizing the null lens. An F/1.5 transmission sphere provides a converging spherical beam to the null lens. The detector is swept through a range that spans paraxial best-focus to marginal best-focus. Note that the transmission sphere is the stop of the system and therefore is also the entrance pupil.

Figure 6 - Photo of the test setup. The transmission sphere (a) provides a converging spherical beam to the null lens being tested (b). A thin, Wratten ND filter (c) is used to reduce the intensity of the beam before it is detected by the camera (d).

Results

Figure 7 shows the measured and retrieved point-spread functions, along with the normalized-mean-squared error between them. Figure 8 shows the estimated wavefront of the system. Figure 9 shows the wavefront predicted by the Zemax model, and the residual error between predicted and estimated wavefronts.

| 0.0444 | 0.1185 | 0.1958 | 0.2666 | 0.2728 | 0.2317 | 0.2098 |

Figure 7 - The measured (top) and retrieved (bottom) PSFs. The left-most image was collected at approximately paraxial best focus. The right-most image was collected at approximately marginal best focus. The distance between each data plane is 5 mm.
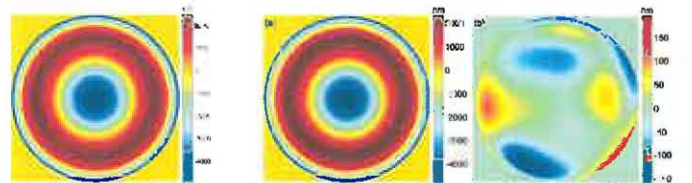

Figure 8 - The estimated wavefront. The RMS value is 2.1 μm.

Figure 9 - (a) The wavefront predicted by the optical model in Zemax. (b) The difference between estimated wavefront and the predicted wavefront. The RMS difference is 50 nm.